EUROPEAN ORGANIZATION FOR NUCLEAR RESEARCH

CERN-PPE/97-14
February 3, 1997

Pair-Production of W Bosons in e^+e^- Interactions at $\sqrt{s} = 161$ GeV

The L3 Collaboration

Abstract

We report on the measurement of W-boson pair-production with the L3 detector at LEP at a centre-of-mass energy of 161.34 GeV. In a data sample corresponding to a total luminosity of 11 pb^{-1}, we select four-fermion events with high invariant masses of pairs of hadronic jets or leptons. Combining all final states, the measured total cross section for W-pair production is: $\sigma_{\mathrm{WW}} = 2.89^{+0.81}_{-0.70}$ (*stat.*) $\pm$ 0.14 (*syst.*) pb. Within the Standard Model, this corresponds to a mass of the W boson of: $\mathrm{M_W} = 80.80^{+0.48}_{-0.42}$ (*exp.*) $\pm$ 0.03 (LEP) GeV. Limits on anomalous triple-vector-boson couplings are derived.

Submitted to *Phys. Lett. B*

1 Introduction

In the first half of the 1996 data taking period, the e^+e^- collider LEP at CERN was operated at a centre-of-mass energy, $\sqrt{s}$, of 161.34 GeV. This centre-of-mass energy coincides with the kinematic threshold of the process $e^+e^- \rightarrow W^+W^-$, thus allowing for the first time the pair-production of $W^\pm$ bosons in e^+e^- interactions. During this run the L3 detector collected a total integrated luminosity of 11 pb^{-1}.

To lowest order, three Feynman diagrams contribute to W-pair production, the s-channel γ and Z-boson exchange and the t-channel ν_e exchange [1], referred to as CC03 [2–4]. The W boson decays into a quark-antiquark pair, for example $W^- \rightarrow \bar{u}d$ or $\bar{c}s$, or a lepton-antilepton pair, $W^- \rightarrow \ell^-\bar{\nu}_\ell$, in the following denoted as qq and $\ell\nu$ for both W^+ and W^- decays. In this article, we report on measurements of all four-fermion final states mediated by W-pair production:

1. $e^+e^- \rightarrow qqe\nu(\gamma)$
2. $e^+e^- \rightarrow qq\mu\nu(\gamma)$
3. $e^+e^- \rightarrow qq\tau\nu(\gamma)$
4. $e^+e^- \rightarrow \ell\nu\ell\nu(\gamma)$
5. $e^+e^- \rightarrow qqqq(\gamma)$,

where (γ) indicates the possible presence of radiative photons.

Additional contributions to the production of these four-fermion final states arise from other neutral-current (NC) or charged-current (CC) Feynman diagrams. For high invariant masses of pairs of fermions and for the visible fermions all within the acceptance of the detector, the additional contributions are small. At the current level of statistical accuracy they need to be taken into account only for $e^+e^- \rightarrow qqe\nu(\gamma)$ (CC20) and $e^+e^- \rightarrow \ell\nu\ell\nu(\gamma)$ (CC56+NC56) [2–4]. The cross-section measurements for the five signal processes are combined to derive the total cross section for W-pair production.

At threshold, these cross sections depend strongly on the centre-of-mass energy and the mass of the W boson, M_W: $\sigma = \sigma(M_W, \sqrt{s})$. From the cross sections as predicted by the Standard Model for this centre-of-mass energy a value for M_W is derived. The s-channel contributions to the cross sections contain the triple-vector-boson vertices γWW and ZWW. Using the independent measurement of the W-boson mass at $p\bar{p}$ colliders [5], the total cross-section measurements allow us to set limits on anomalous triple-vector-boson couplings.

2 The L3 Detector

The L3 detector [6] consists of a silicon micro-strip detector [7], a central tracking chamber, a high-resolution electromagnetic calorimeter composed of BGO crystals, a lead-scintillator ring calorimeter at low polar angles [8], a scintillation counter system, a uranium hadron calorimeter with proportional wire chamber readout, and an accurate muon chamber system. A forward-backward muon detection system extends the polar angle coverage of the muon chambers down to 24 degrees in the forward-backward region [9]. These detectors are installed in a 12 m diameter magnet which provides a solenoidal field of 0.5 T and a toroidal field of 1.2 T. The luminosity is measured using BGO calorimeters [10] situated on each side of the detector.

The response of the L3 detector is modelled with the GEANT [11] detector simulation program which includes the effects of energy loss, multiple scattering and showering in the detector materials and in the beam pipe.

3 Measurement of Four-Fermion Production

The analyses described below reconstruct the four-fermion final states. Charged leptons are explicitly identified using their characteristic signature. Hadronic jets are reconstructed by combining calorimetric energy depositions using the Durham jet algorithm [12]. Calorimetric clusters are treated as massless and are combined adding their four-momenta. The momentum of the neutrino in $qq\ell\nu$ events is identified with the missing momentum vector.

Selection efficiencies and background contaminations of all processes are determined by Monte Carlo simulations. The following Monte Carlo event generators are used to simulate the various signal and background reactions: KORALW [13] ($e^+e^- \rightarrow WW \rightarrow ffff(\gamma)$); EXCALIBUR [14] ($e^+e^- \rightarrow ffff(\gamma)$); PYTHIA [15] ($e^+e^- \rightarrow q\bar{q}(\gamma), ZZ(\gamma)$, hadronic two-photon collisions); KORALZ [16] ($e^+e^- \rightarrow \mu^+\mu^-(\gamma),\ \tau^+\tau^-(\gamma)$); BHAGENE3 [17] ($e^+e^- \rightarrow e^+e^-(\gamma)$).

Systematic errors on the cross-section measurements are conservative estimates and in all cases small compared to the statistical error. The measurement of the total luminosity, $\mathcal{L}$, follows the procedure described in [18, 19]. The total error on the luminosity measurement is estimated to be 0.6% [19].

The results on cross sections and couplings are determined in a combined fit as discussed in Section 4.

3.1 $e^+e^- \rightarrow qqe\nu(\gamma)$

Event Selection

The event selection for the process $e^+e^- \rightarrow qqe\nu(\gamma)$ requires an identified electron, missing momentum due to the neutrino, and high multiplicity arising from the qq system. A $qqe\nu$ event selected in the data is shown in Figure 1.

The electron is identified in the electromagnetic calorimeter as the highest energy deposition with electromagnetic shower shape. This calorimetric cluster must have a polar angle of $|\cos\theta_e| < 0.90$ and an energy E_e larger than 25 GeV. In order to reject radiative photons, a track in the central tracking chamber must match the electron cluster within 10 mrad in azimuth. Electrons arising from decays of hadrons are rejected by requiring the electron to be isolated from the hadronic system. Isolation is imposed by asking that the electron energy is at least 70% of the total calorimetric energy deposited in a cone of half opening angle 15 degrees around the electron direction.

The neutrino energy E_ν, inferred from the missing momentum of the event, must be larger than 25 GeV. In order to reject radiative $q\bar{q}(\gamma)$ events where the photon escapes along the beam pipe, the polar angle of the missing momentum vector must point well inside the detector, $|\cos\theta_\nu| < 0.90$.

The hadronic system is characterised by a large particle multiplicity. Requiring at least 15 calorimetric clusters rejects all purely leptonic final states. After having removed the calorimetric energy depositions associated with the identified electron, the remaining calorimetric clusters are grouped into two jets. The masses of the two W bosons are calculated as the invariant masses of the electron-neutrino system, $M_{e\nu}$, and the jet-jet system, M_{qq}. Both invariant masses are required to be larger than 50 GeV.

The distributions of the electron energy and of the invariant mass of the electron-neutrino system are shown in Figure 2, comparing data to Monte Carlo.

Cross Section

The above cuts select four events in the data. The selection efficiencies and the background contributions are listed in Table 1. The signal efficiency is determined within the following cuts: $E_\mathrm{e}, E_\nu > 25$ GeV; $|\cos\theta_\mathrm{e}|, |\cos\theta_\nu| < 0.90$; $M_{\mathrm{e}\nu}, M_{qq} > 50$ GeV. The accepted background cross section is dominated by the processes $\mathrm{e^+e^-} \rightarrow q\bar{q}(\gamma)$ and $\mathrm{e^+e^-} \rightarrow q\bar{q}\mathrm{e^+e^-}$ when one of the leptons escapes detection.

Systematic errors in the electron identification are derived from a comparison of data versus Monte Carlo using $\mathrm{e^+e^-} \rightarrow \mathrm{e^+e^-}(\gamma)$ events as a control sample. Systematic errors on efficiencies and accepted background cross sections are derived by comparing different Monte Carlo event generators and Monte Carlo samples simulated with different W masses and detector energy scales. A total systematic error of 5% on the measured cross section of the reaction $\mathrm{e^+e^-} \rightarrow qq\mathrm{e}\nu(\gamma)$ within the above cuts is assigned.

3.2 $\mathrm{e^+e^-} \rightarrow qq\mu\nu(\gamma)$

Event Selection

The event selection for the process $\mathrm{e^+e^-} \rightarrow qq\mu\nu(\gamma)$ requires an identified muon, missing momentum due to the neutrino, and high multiplicity arising from the qq system.

The muon is identified in the muon spectrometer as the highest momentum track pointing back to the interaction vertex. It must have a momentum larger than 20 GeV. Muons arising from decays of hadrons are rejected by requiring the muon to have an angular separation of at least 15 degrees to both hadronic jets reconstructed as described below. In order to reject $q\bar{q}\mu^+\mu^-$ events, any additional muon reconstructed in the muon chambers must have a momentum of less than 20 GeV.

The neutrino direction is inferred from the missing momentum direction of the event. In order to reject radiative $q\bar{q}(\gamma)$ events where the photon escapes along the beam pipe, the polar angle of the missing momentum vector must point inside the detector, $|\cos\theta_\nu| < 0.95$. Requiring at least 15 calorimetric clusters and at least five tracks in the central tracking chamber rejects all purely leptonic final states as well as cosmic-ray background.

The calorimetric clusters are grouped into two jets. The masses of the two W bosons are calculated as the invariant masses of the muon-neutrino system and the jet-jet system. The muon-neutrino invariant mass must be larger than 55 GeV, and the jet-jet invariant mass must be larger than 40 GeV and smaller than 120 GeV.

The distributions of the angle between the muon and the nearest jet and of the invariant mass of the muon-neutrino system are shown in Figure 3.

Cross Section

The above cuts select four events in the data. The selection efficiencies and the background contributions are listed in Table 1. The accepted background cross section is dominated by the processes $\mathrm{e^+e^-} \rightarrow q\bar{q}(\gamma)$ and $\mathrm{e^+e^-} \rightarrow q\bar{q}\mu^+\mu^-$ when one of the leptons escapes detection.

Systematic errors are evaluated as described above. A total systematic error of 5% on the measured cross section is assigned.

3.3 $e^+e^- \to qq\tau\nu(\gamma)$

Event Selection

The event selection for the process $e^+e^- \to qq\tau\nu(\gamma)$ is based on the identification of a tau jet in a hadronic event, combined with missing energy. The tau jet is identified as a low-energy electron or muon, or a low-multiplicity narrow jet, isolated from the rest of the event.

Events are selected on the basis of the final-state particle multiplicity. Events must have more than 15 calorimetric clusters, rejecting low-multiplicity leptonic final states. High-multiplicity purely hadronic final states are rejected by a cut in the two-dimensional plane spanned by the number of tracks reconstructed in the central tracking chamber and the number of calorimetric clusters.

Requirements on the missing energy and momentum are imposed. Signal events contain at least two neutrinos, resulting in missing momentum and reduced visible energy. In order to reject $q\bar{q}(\gamma)$ and $qqqq(\gamma)$ events the difference between the visible energy and the missing momentum must be less than 120 GeV. Requiring the longitudinal energy imbalance to be smaller than 30 GeV and the transverse energy imbalance to be larger than 5 GeV suppresses $q\bar{q}(\gamma)$ events with hard initial-state radiation.

The tau lepton is identified by its decay products. Electrons and muons are identified according to the lepton identification described above. If the lepton energy is larger than 5 GeV and the sum of the lepton energy and the missing momentum less than 65 GeV, the identified electron or muon is considered as the tau jet.

If no electrons or muons are found, geometrical jets are reconstructed based on clustering inside a cone of 15 degrees half-opening angle. At least three jets with an energy larger than 10 GeV are required. Out of the three most energetic jets the two most back-to-back jets are associated with the qq system. The most energetic remaining jet is taken as the tau jet. The efficiency of this tau jet identification for hadronic tau decays is 83%. In order to reduce the background coming from $qqe\nu(\gamma)$ events with the electron not identified, events with the tau jet having more than 35 GeV of energy deposited in the electromagnetic calorimeter and less than 3 GeV in the hadron calorimeter are rejected. The background of $qq\mu\nu(\gamma)$ events with the muon not identified in the muon chambers is reduced by rejecting events where the tau jet is compatible with a minimum-ionising particle.

The tau jet must contain one, two or three tracks reconstructed in the central tracking chamber. After having removed the tracks and calorimetric energy depositions associated with the identified tau jet, the remaining tracks and calorimetric clusters are grouped into two hadronic jets using the Durham jet algorithm. The tau jet must be separated by at least 25 degrees from the two hadronic jets. For events with a transverse energy imbalance less than 25 GeV and with $|\cos\theta_{miss}| > 0.55$ for the polar angle of the missing momentum vector, the angular opening of the tau jet must be smaller than eight degrees. The invariant mass of the system of the two hadronic jets must be larger than 60 GeV and smaller than 100 GeV. The invariant mass of the system of the tau jet and the missing four-momentum must be larger than 55 GeV.

The distributions of the number of tracks reconstructed in the central tracking chamber and associated with the tau jet and of the invariant mass of the two hadronic jets are shown in Figure 4.

Cross Section

The above cuts select three events in the data. The selection efficiencies and the background contributions are listed in Table 1. The accepted background cross section is dominated by the process $e^+e^- \to q\bar{q}(\gamma)$.

The dominant systematic error on the signal cross section arises from the uncertainty in the accepted $q\bar{q}(\gamma)$ background cross section which is dominated by finite Monte Carlo statistics and leads to a relative error of 19% on the signal cross section. Systematic errors in the tau-jet identification are derived from a comparison of data versus Monte Carlo using $e^+e^- \to \tau^+\tau^-(\gamma)$ events as a control sample. Systematic errors on efficiencies and accepted background cross sections are derived by comparing different Monte Carlo event generators and Monte Carlo samples simulated with different W masses and detector energy scales. A total systematic error of 20% on the measured cross section is assigned.

3.4 $e^+e^- \to \ell\nu\ell\nu(\gamma)$

Event Selection

The event selection for the process $e^+e^- \to \ell\nu\ell\nu(\gamma)$ requires two leptons and missing energy due to the neutrinos. Low-multiplicity leptonic final states are selected by requiring between one and six tracks in the central tracking chamber and less than 15 calorimetric clusters. The visible energy of the event is required to be larger than 2% and smaller than 80% of $\sqrt{s}$.

Charged leptons are identified inside the polar angular range of $|\cos\theta| < 0.92$. For electrons and muons, the lepton identification as described above is applied. For muons not reconstructed in the muon chambers, their minimum-ionising-particle (MIP) signature in the calorimeters is used for identification. Final states from hadronic tau decays are identified as geometrical jets which are reconstructed based on a clustering inside a cone of 30 degrees half-opening angle. At least one identified electron or muon with an energy between 20 GeV and 70 GeV is required. The selection criteria depend on whether one or two electrons or muons are identified, referred to in the following as lepton-jet and lepton-lepton class.

In the lepton-lepton class, the energy of the second lepton must be larger than 8 GeV and smaller than 70 GeV. In order to reject $\ell^+\ell^-(\gamma)$ events, the acoplanarity between the two leptons is required to be larger than eight degrees. Exactly two tracks must be reconstructed in the central tracking chamber. The transverse energy imbalance must be at least 8 GeV and larger than 10% of the visible energy. In order to reject radiative $\ell^+\ell^-(\gamma)$ events where the photon escapes along the beam pipe, the polar angle of the missing momentum vector must neither point to the beam axis, $|\cos\theta_{miss}| < 0.96$, nor to the gap between the barrel and endcap electromagnetic calorimeter. The calorimetric energy not associated with the leptons is required to be less than 10 GeV, and the sum of the energies of jets with $|\cos\theta_{jet}| > 0.95$ must be less than 5 GeV.

In the lepton-jet class, a jet with more than 8 GeV energy is required. In order to reject $\ell^+\ell^-(\gamma)$ events the acoplanarity between the lepton and the jet as well as between the lepton and any track in the central tracking chamber must be larger than eight degrees. At least one track is required to have a momentum larger than 2 GeV. The missing transverse energy must exceed 20% of the visible energy. Since for muons identified by their MIP signature the momentum resolution is worse, the missing energy vector is required to point at least 23 degrees in polar angle away from the MIP muon. Events containing photons with an energy of more than 10 GeV are rejected.

The distributions of the acoplanarity between the two charged leptons and of the energy of the identified electron or muon with highest energy are shown in Figure 5.

Cross Section

The above selection cuts select two events in the data, one electron-muon event in the lepton-lepton class, and one muon-tau event in the lepton-jet class. The combined selection efficiencies and the background contributions are listed in Table 1. The signal efficiency is determined within the following cuts: $|\cos\theta| < 0.96$ for both charged leptons, with energies larger than 15 GeV and 5 GeV. The accepted background cross section is dominated by $e^+e^-(\gamma)$ and $\mu^+\mu^-(\gamma)$ events.

The dominant systematic error on the signal cross section arises from the uncertainty of 6 fb in the accepted $\ell^+\ell^-(\gamma)$ background cross section due to finite Monte Carlo statistics. Systematic errors on the lepton identification are derived from a comparison of data versus Monte Carlo using $e^+e^- \to \ell^+\ell^-(\gamma)$ events as a control sample. Systematic errors on efficiencies and accepted background cross sections are derived by comparing different Monte Carlo event generators and Monte Carlo samples simulated with different W masses and detector energy scales. A total systematic error of 5% on the measured cross section is assigned.

3.5 $e^+e^- \to qqqq(\gamma)$

Event Selection

The event selection for the process $e^+e^- \to qqqq(\gamma)$ requires a four-jet signature, with kinematics compatible with a WW intermediate state. The main background arises from the process $e^+e^- \to q\bar{q}(\gamma)$, which can lead to multi-jet final states through gluon radiation and jet reconstruction and has a total cross section about two orders of magnitude larger than the expected signal.

Events with high multiplicity and no missing energy are selected by requiring at least five tracks in the central tracking chamber, at least 30 calorimetric clusters and a visible energy larger than $0.65\sqrt{s}$. Requiring the longitudinal energy imbalance normalised to the visible energy to be smaller than 0.25 and rejecting events which contain an electromagnetic cluster with an energy of more than 30 GeV suppresses $q\bar{q}(\gamma)$ events with hard initial-state radiation.

Selected events are clustered with a variable jet-resolution parameter such that four jets are formed. The jet resolution parameter at which the event changes from a four-jet to a three-jet topology, Y_{34}, must be larger than 0.0025, selecting events with four well separated jets. The determination of the jet energies and angles is improved by a kinematic fit imposing four-momentum conservation. This selection accepts 88.4% of the WW $\to qqqq(\gamma)$ signal while reducing the dominating $q\bar{q}(\gamma)$ background by a factor of 21. A total of 80 events pass this selection.

Two pairs of jets are formed, corresponding to the two W bosons. The chosen jet-jet pairing maximizes the sum of the two jet-jet invariant masses, which yields the correct assignment for about 80% of the selected WW $\to qqqq(\gamma)$ events.

Because of the very high $q\bar{q}(\gamma)$ background and the similar topology of four-jet events arising in WW and $q\bar{q}$ production, a neural network is used to improve their separation. A three-layer feed-forward neural network [20] with twelve input nodes, one hidden layer with 15 nodes, and one output node is trained on signal and background Monte Carlo such that the output peaks at 1 for the signal, and at 0 for the background. The twelve input variables consist of event shape variables sensitive to the general four-jet topology (Y_{34}, sphericity, minimal and maximal jet energy, minimal cluster multiplicity of the four jets), to the signal kinematics (sum and difference of the two W masses and W velocities, maximal acollinearity between jets belonging to the same W), and to the background topology (minimal angle between jets, minimal mass of jets when the event is reconstructed as a two-jet event).

The distributions of the jet resolution parameter Y_{34} and of the sum of the two jet-jet masses are shown in Figure 6. The distribution of the neural-network output is shown in Figure 7. All selection cuts have been applied. An alternative analysis not based on a neural network yields compatible but less precise results.

Cross Section

The output of the neural network for data events is fitted by a linear combination of neural-network output distributions derived from Monte Carlo simulations for signal and background. A maximum-likelihood fit [21] is used to determine the fraction of $qqqq(\gamma)$ signal events in the total sample of selected events. The cross sections of all background processes other than $q\bar{q}(\gamma)$, corresponding to 2.3 events of the selected 80 events, are fixed to their Standard-Model expectations. This allows a determination of the fraction of $q\bar{q}(\gamma)$ events in the accepted sample.

Taking selection efficiencies and luminosity into account, the result of the fit corresponds to a signal cross section of $0.98^{+0.51}_{-0.40}$ pb and a $q\bar{q}(\gamma)$ cross section of 142^{+19}_{-18} pb where the errors are statistical. The measured $q\bar{q}(\gamma)$ cross section is in good agreement with both our dedicated measurements of fermion-pair cross sections and with the Standard Model value [19].

The largest systematic error arises from differences between data and Monte Carlo distributions for the neural-network input variables. Decreasing these differences by a reweighting procedure changes the signal cross section by 4%, which is taken as a systematic error. This error is dominated by the effect of reweighting $q\bar{q}(\gamma)$ Monte Carlo events as a function of Y_{34} derived from a comparison of data versus Monte Carlo at 91 GeV centre-of-mass energy. Systematic errors due to the variation of the W mass used in the Monte Carlo simulations and different detector energy scales are estimated to be less than 3%. The effect of an imperfect simulation of cluster multiplicities is estimated to be less than 2%. A total systematic error of 5% on the measured cross section is assigned.

4 Results

Signal Cross Sections

The cross sections, σ_i, of the signal processes i are determined simultaneously in one maximum-likelihood fit. The total likelihood is given by the product of Poissonian probabilities, $P(N_i, \mu_i)$, corresponding to the signal processes i having N_i selected events (Table 2). The expected number of events for process i, μ_i, is calculated as:

$$\mu_i \;=\; \left(\sum_{j=1}^{5} \epsilon_{ij}\sigma_j + \sigma_i^{\mathrm{bg}} \right) \cdot \mathcal{L}_i \;, \qquad (1)$$

where ϵ_{ij} is the efficiency of selection i to accept events from process j, σ_i^{bg} is the remaining background cross section arising from other processes, and $\mathcal{L}_i$ is the luminosity used in the analysis of process i. These numbers are listed in Tables 1 and 2. For the $\mathrm{e}^+\mathrm{e}^- \to qqqq(\gamma)$ process, the Poissonian probability is replaced by the likelihood as a function of the signal cross section derived from the fit described in Section 3.5. Statistical errors corresponding to a 68% confidence level interval are determined by a change of 0.5 in the logarithm of the total likelihood. The resulting cross sections and their statistical errors as given by the fit are listed in Table 2.

For the $qqe\nu(\gamma)$ and $\ell\nu\ell\nu(\gamma)$ final state the measured cross sections contain significant contributions from processes not mediated by resonant W-pair production. In order to determine W-pair cross sections also for these final states the measured cross sections are scaled by a multiplicative factor, f_i. These conversion factors are given by the ratio of the total CC03 cross section and the four-fermion cross section within cuts, and are calculated within the Standard Model using the EXCALIBUR [14] event generator. They are determined to be 1.27 for $qqe\nu(\gamma)$ and 0.92 for $\ell\nu\ell\nu(\gamma)$, where the dependence of the f_i on $\mathrm{M_W}$ is negligible. These cross sections for the $qqe\nu(\gamma)$ and $\ell\nu\ell\nu(\gamma)$ final states are also listed in Table 2.

W-Pair Cross Section and W-Decay Branching Fractions

For the determination of the total CC03 production cross section of W-pairs, σ_{WW}, the ansatz described above is modified. The channel cross sections σ_i are replaced by the product $r_i\sigma_{\mathrm{WW}}$ or $r_i\sigma_{\mathrm{WW}}/f_i$ for the $qqe\nu(\gamma)$ and $\ell\nu\ell\nu(\gamma)$ final states. The ratio r_i is the ratio between the CC03 cross section for process i and σ_{WW}. They are given in terms of the W-decay branching fractions, $B(\mathrm{W}\rightarrow qq)$ and $B(\mathrm{W}\rightarrow \ell\nu)$, as follows: $r_{qqqq} = [B(\mathrm{W}\rightarrow qq)]^2$, $r_{qq\ell\nu} = 2B(\mathrm{W}\rightarrow qq)B(\mathrm{W}\rightarrow \ell\nu)$, and $r_{\ell\nu\ell\nu} = [1 - B(\mathrm{W}\rightarrow qq)]^2$, where the sum of the hadronic and the three leptonic branching fractions is constrained to be unity.

The total W-pair cross section and the W-decay branching fractions as determined from fits to the data are listed in Table 3. They are determined both with and without the assumption of charged-current lepton universality in W decays. The W-decay branching fractions obtained for the individual leptons are in agreement with each other. This is the first direct determination of the branching fraction of the W to hadrons. In order to obtain an improved determination of σ_{WW}, the W-decay branching fractions from the Standard Model are imposed, which are calculated including QCD and mass corrections [3] (Table 3). The result for the total production cross section of W-pairs at $\sqrt{s} = 161.34 \pm 0.06$ GeV [22] is:

$$\sigma_{\mathrm{WW}} = 2.89^{+0.81}_{-0.70}\ (stat.) \pm 0.14\ (syst.)\ \mathrm{pb}\ , \qquad (2)$$

where the first error is statistical and the second systematic. This value for σ_{WW} agrees well with other recent measurements of σ_{WW} at $\sqrt{s} = 161$ GeV [23, 24].

W Mass

Within the Standard Model the measured cross sections, σ_i, depend on $\sqrt{s}$ and the mass of the W boson, $\mathrm{M_W}$. In order to determine a value for $\mathrm{M_W}$, the cross-section fit to the data is repeated with the cross sections σ_i of Equation 1 replaced by the functions $\sigma_i(\sqrt{s}, \mathrm{M_W})$, leaving $\mathrm{M_W}$ as the only free parameter. Using the Standard-Model calculations of $\sigma_i(\sqrt{s}, \mathrm{M_W})$ as implemented in GENTLE [25] (CC03) and EXCALIBUR [14] ($qqe\nu(\gamma)$ and $\ell\nu\ell\nu(\gamma)$ final states), $\mathrm{M_W}$ is found to be:

$$\mathrm{M_W} = 80.80^{+0.48}_{-0.42}\ (exp.) \pm 0.03\ (\mathrm{LEP})\ \ \mathrm{GeV}\ .$$

The same result for $\mathrm{M_W}$ is obtained using only the total W-pair cross section of Equation 2, as shown in Figure 8. The second error on $\mathrm{M_W}$ arises from the uncertainty in the calibration of the LEP beam energy [22]. The error due to the experimental uncertainty of the total W-boson width [26] is negligible. This value for $\mathrm{M_W}$ agrees well with our indirect determination of $\mathrm{M_W}$ from measurements at the Z resonance [18], and with recent measurements of $\mathrm{M_W}$ at $\mathrm{p\bar{p}}$ colliders [5, 27] and at LEP [23, 24].

Triple-Vector-Boson Couplings

Alternatively, when the W mass is known, the total cross section can be interpreted in terms of triple-vector-boson couplings [28, 29]. In particular, it is interesting to test if the coupling between the Z and a pair of W bosons exists [30]. In general, anomalous contributions to W-pair production are parametrised in terms of seven complex triple-vector-boson couplings, too many to be measured with the limited data collected at threshold. Therefore scenarios are considered where a single parameter describes a possible deviation from the couplings predicted by the Standard Model.

Neglecting the contributions of dimension-six operators, assuming that all electromagnetic properties of the W boson are standard and that a SU(2) symmetry is respected leaves a single parameter, δ_Z [30]. This parameter describes the deviation of the ZWW coupling, g_ZWW, from its Standard Model value of $\cot\theta_\mathrm{W} = 1.9$, where θ_W is the electroweak mixing angle. Our result is:

$$\begin{aligned}\delta_\mathrm{Z} &= g_\mathrm{ZWW} - \cot\theta_\mathrm{W} \\ &= -0.1 \pm 1.9 \quad (68\%\ \mathrm{CL}) \\ &= -0.1 \pm 3.2 \quad (95\%\ \mathrm{CL})\ ,\end{aligned}$$

as shown in Figure 9. Thus our cross section is in good agreement with the Standard Model predictions for the triple-vector-boson couplings and our data favour the existence of the ZWW vertex at about 68% confidence level. In an alternative scenario [29], where more than one anomalous coupling is introduced, but depending on a single parameter, $\alpha_{\mathrm{W}\Phi}$, one finds:

$$\begin{aligned}\alpha_{\mathrm{W}\Phi} &= 0.0 \pm 0.8 \quad (68\%\ \mathrm{CL}) \\ &= 0.0 \pm 1.4 \quad (95\%\ \mathrm{CL})\ ,\end{aligned}$$

as also shown in Figure 9. This value for $\alpha_{\mathrm{W}\Phi}$ agrees well with other recent measurements of $\alpha_{\mathrm{W}\Phi}$ at LEP [24, 31].

In order to derive these results with a maximum likelihood fit, the GENTLE [25] program is used to calculate the prediction for the total cross sections as a function of the anomalous coupling, using Standard Model W-decay branching fractions and the current world-average value and error for the W mass, 80.33 ± 0.15 GeV [5]. The errors quoted above include the contributions due to the error on the world-average value of the W mass and the systematic errors of the cross section measurements. In both scenarios good agreement with the Standard Model expectation of $\delta_\mathrm{Z} = \alpha_{\mathrm{W}\Phi} = 0$ is observed. Limits on other anomalous triple-vector-boson couplings are also obtained from measurements at $\mathrm{p\bar{p}}$ colliders [32].

5 Summary and Conclusion

In a data sample corresponding to an integrated luminosity of 11 pb^{-1} collected at a centre-of-mass energy of 161.34 GeV, we have measured W-pair production by selecting four-fermion events with high invariant masses. All final states mediated by W-pair production are analysed.

The total W-pair cross section is found to be $2.89^{+0.81}_{-0.70}$ (*stat.*) $\pm$ 0.14 (*syst.*) pb. Within the Standard Model, this cross section corresponds to a W-boson mass of $80.80^{+0.48}_{-0.42}$ (*exp.*) $\pm$ 0.03 (LEP) GeV. Alternatively, using an independent determination of the W-mass [5], the cross-section measurement favours the existence of the ZWW vertex; limits on anomalous triple-vector-boson couplings are $|\delta_Z| < 3.2$ or $|\alpha_{W\Phi}| < 1.4$ at 95% CL.

6 Acknowledgements

We wish to congratulate the CERN accelerator divisions for the successful upgrade of the LEP machine and to express our gratitude for its good performance. We acknowledge with appreciation the effort of all engineers, technicians and support staff who have participated in the construction and maintenance of this experiment. Those of us who are not from member states thank CERN for its hospitality and help. We also thank D. Schildknecht for useful discussions.

References

[1] S. L. Glashow, Nucl. Phys. **22** (1961) 579;
S. Weinberg, Phys. Rev. Lett. **19** (1967) 1264;
A. Salam, “Elementary Particle Theory”, ed. N. Svartholm, Stockholm, “Almquist and Wiksell” (1968), 367.

[2] D. Bardin *et al.*, Nucl. Phys. (Proc. Suppl.) **B 37** (1994) 148;
F.A. Berends *et al.*, Nucl. Phys. (Proc. Suppl.) **B 37** (1994) 163.

[3] W. Beenakker *et al.*, in *Physics at LEP 2*, Report CERN 96-01 (1996), eds G. Altarelli, T. Sjöstrand, F. Zwirner, Vol. 1, p. 79.

[4] D. Bardin *et al.*, in *Physics at LEP 2*, Report CERN 96-01 (1996), eds G. Altarelli, T. Sjöstrand, F. Zwirner, Vol. 2, p. 3.

[5] The UA1 Collaboration, C. Albajar *et al.*, Z. Phys. **C 44** (1989) 15;
The UA2 Collaboration, J. Alitti *et al.*, Phys. Lett. **B 241** (1990) 150; Phys. Lett. **B 276** (1992) 354;
The CDF Collaboration, F. Abe *et al.*, Phys. Rev. Lett. **65** (1990) 2243; Phys. Rev. **D 43** (1991) 2070; Phys. Rev. Lett. **75** (1995) 11; Phys. Rev. **D 52** (1995) 4784;
The DØ Collaboration, S. Abachi *et al.*, Phys. Rev. Lett. **77** (1996) 3309.
We use the average value and error for the mass of the W boson as listed in:
R.M. Barnett *et al.*, *Review of Particle Properties*, Phys. Rev. **D 54** (1996) 1.

[6] The L3 Collaboration, B. Adeva *et al.*, Nucl. Instr. and Meth. **A 289** (1990) 35.

[7] M. Acciarri *et al.*, Nucl. Instr. and Meth. **A 351** (1994) 300.

[8] M. Chemarin *et al.*, Nucl. Instr. and Meth. **A 349** (1994) 345.

[9] A. Adam *et al.*, *The Forward Muon Detector of L3*, CERN-PPE/96-097.

[10] I.C. Brock *et al.*, Nucl. Instr. and Meth. **A 381** (1996) 236.

[11] The L3 detector simulation is based on GEANT Version 3.15.
R. Brun *et al.*, *GEANT 3*, CERN-DD/EE/84-1 (Revised), 1987.
The GHEISHA program (H. Fesefeldt, RWTH Aachen Report PITHA 85/02 (1985)) is used to simulate hadronic interactions.

[12] S. Catani *et al.*, Phys. Lett. **B 269** (1991) 432.

[13] The KORALW version 1.21 is used.
M. Skrzypek, S. Jadach, W. Placzek and Z. Wąs, Comp. Phys. Comm. **94** (1996) 216;
M. Skrzypek, S. Jadach, M. Martinez, W. Placzek and Z. Wąs, Phys. Lett. **B 372** (1996) 289.

[14] F.A. Berends, R. Kleiss and R. Pittau, Nucl. Phys. **B 424** (1994) 308; Nucl. Phys. **B 426** (1994) 344; Nucl. Phys. (Proc. Suppl.) **B 37** (1994) 163; Phys. Lett. **B 335** (1994) 490;
R. Kleiss and R. Pittau, Comp. Phys. Comm. **83** (1994) 141.

[15] T. Sjöstrand, *PYTHIA 5.7 and JETSET 7.4 Physics and Manual*, CERN-TH/7112/93 (1993), revised August 1995;
T. Sjöstrand, Comp. Phys. Comm. **82** (1994) 74.

[16] The KORALZ version 4.01 is used.
S. Jadach, B. F. L. Ward and Z. Wąs, Comp. Phys. Comm. **79** (1994) 503.

[17] J. H. Field, Phys. Lett. **B 323** (1994) 432;
J. H. Field and T. Riemann, Comp. Phys. Comm. **94** (1996) 53.

[18] The L3 Collaboration, M. Acciarri *et al.*, Z. Phys. **C 62** (1994) 551.

[19] The L3 Collaboration, *Measurement of Hadron and Lepton-Pair Production at 161 GeV* $< \sqrt{s} <$ *172 GeV at LEP*, in preparation.

[20] C. Peterson *et al.*, Comp. Phys. Comm. **81** (1994) 185.

[21] R. Barlow, J. Comp. Phys. **72** (1987) 202;
R. Barlow and Ch. Beeston, Comp. Phys. Comm. **77** (1993) 219.

[22] The working group on LEP energy, CERN-SL note, in preparation.

[23] The OPAL Collaboration, K. Ackerstaff *et al.*, Phys. Lett. **B 389** (1996) 416.

[24] The DELPHI Collaboration, P. Abreu *et al.*, *Measurement and interpretation of the W-pair cross-section in* e^+e^- *interactions at 161 GeV*, CERN-PPE/97-09.

[25] The GENTLE version 2.0 is used.
D. Bardin *et al.*, *GENTLE/4fan v. 2.0: A Program for the Semi-Analytic Calculation of Predictions for the Process* $e^+e^- \to 4f$, DESY 96-233, hep-ph/9612409.

[26] The UA1 Collaboration, C. Albajar *et al.*, Phys. Lett. **B 253** (1991) 503;
The UA2 Collaboration, J. Alitti *et al.*, Phys. Lett. **B 276** (1992) 365;
The CDF Collaboration, F. Abe *et al.*, Phys. Rev. Lett. **74** (1995) 341; Phys. Rev. **D 52** (1995) 2624;
The DØ Collaboration, S .Abachi *et al.*, Phys. Rev. Lett. **75** (1995) 1456.
We use the average value and error for the total width of the W boson as listed in:
R.M. Barnett *et al.*, *Review of Particle Properties*, Phys. Rev. **D 54** (1996) 1.

[27] M. Rijssenbeek, *Measurements of the Mass of the W Boson from CDF/DØ*, to appear in the proceedings of the 28th International Conference on High Energy Physics, 25-31 July 1996, Warsaw, Poland.

[28] K. Hagiwara *et al.*, Nucl. Phys. **B 282** (1987) 253.

[29] G. Gounaris *et al.*, in *Physics at LEP 2*, Report CERN 96-01 (1996), eds G. Altarelli, T. Sjöstrand, F. Zwirner, Vol. 1, p. 525.

[30] I. Kuss and D. Schildknecht, Phys. Lett. **B 383** (1996) 470.

[31] The OPAL Collaboration, K. Ackerstaff *et al.*, *Measurement of the triple gauge boson coupling* $\alpha_{W\Phi}$ *from* W^+W^- *production in* e^+e^- *collisions at* $\sqrt{s} = 161$ *GeV*, CERN-PPE/97-04.

[32] The UA2 Collaboration, J. Alitti *et al.*, Phys. Lett. **B 277** (1992) 194;
The CDF Collaboration, F. Abe *et al.*, Phys. Rev. Lett. **75** (1995) 1017;
The DØ Collaboration, S .Abachi *et al.*, Phys. Rev. Lett. **75** (1995) 1023; Phys. Rev. Lett. **75** (1995) 1034; Phys. Rev. Lett. **77** (1996) 3303.

The L3 Collaboration:

M.Acciarri,[29] O.Adriani,[18] M.Aguilar-Benitez,[28] S.Ahlen,[12] B.Alpat,[36] J.Alcaraz,[28] G.Alemanni,[24] J.Allaby,[19] A.Aloisio,[31] G.Alverson,[13] M.G.Alviggi,[31] G.Ambrosi,[21] H.Anderhub,[51] V.P.Andreev,[7,40] T.Angelescu,[14] F.Anselmo,[10] D.Antreasyan,[10] A.Arefiev,[30] T.Azemoon,[3] T.Aziz,[11] P.Bagnaia,[39] L.Baksay,[46] S.Banerjee,[11] K.Banicz,[48] R.Barillère,[19] L.Barone,[39] P.Bartalini,[36] A.Baschirotto,[29] M.Basile,[10] R.Battiston,[36] A.Bay,[24] F.Becattini,[18] U.Becker,[17] F.Behner,[51] J.Berdugo,[28] P.Berges,[17] B.Bertucci,[19] B.L.Betev,[51] S.Bhattacharya,[11] M.Biasini,[19] A.Biland,[51] G.M.Bilei[36] J.J.Blaising,[19] S.C.Blyth,[37] G.J.Bobbink,[2] R.Bock,[1] A.Böhm,[1] B.Borgia,[39] D.Bourilkov,[51] M.Bourquin,[21] S.Braccini,[21] J.G.Branson,[42] V.Brigljevic,[51] I.C.Brock,[37] A.Buffini,[18] A.Buijs,[47] J.D.Burger,[17] W.J.Burger,[21] J.Busenitz,[46] A.Button,[3] X.D.Cai,[17] M.Campanelli,[51] M.Capell,[17] G.Cara Romeo,[10] M.Caria,[36] G.Carlino,[31] A.M.Cartacci,[18] J.Casaus,[28] G.Castellini,[18] F.Cavallari,[39] N.Cavallo,[31] C.Cecchi,[21] M.Cerrada,[28] F.Cesaroni,[25] M.Chamizo,[28] A.Chan,[53] Y.H.Chang,[53] U.K.Chaturvedi,[20] S.V.Chekanov,[33] M.Chemarin,[27] A.Chen,[53] G.Chen,[8] G.M.Chen,[8] H.F.Chen,[22] H.S.Chen,[8] X.Chereau,[4] G.Chiefari,[31] C.Y.Chien,[5] M.T.Choi,[45] L.Cifarelli,[41] F.Cindolo,[10] C.Civinini,[18] I.Clare,[17] R.Clare,[17] H.O.Cohn,[34] G.Coignet,[4] A.P.Colijn,[2] N.Colino,[28] V.Commichau,[1] S.Costantini,[33] F.Cotorobai,[14] B.de la Cruz,[28] A.Csilling,[15] T.S.Dai,[17] R.D'Alessandro,[18] R.de Asmundis,[31] A.Degré,[4] K.Deiters,[49] D.della Volpe,[31] P.Denes,[38] F.DeNotaristefani,[39] D.DiBitonto,[46] M.Diemoz,[39] D.van Dierendonck,[2] F.Di Lodovico,[51] C.Dionisi,[39] M.Dittmar,[51] A.Dominguez,[42] A.Doria,[31] M.T.Dova,[20,♯] E.Drago,[31] D.Duchesneau,[4] P.Duinker,[2] I.Duran,[43] S.Dutta,[11] S.Easo,[36] Yu.Efremenko,[34] H.El Mamouni,[27] A.Engler,[37] F.J.Eppling,[17] F.C.Erné,[2] J.P.Ernenwein,[27] P.Extermann,[21] M.Fabre,[49] R.Faccini,[39] S.Falciano,[39] A.Favara,[18] J.Fay,[27] O.Fedin,[40] M.Felcini,[51] B.Fenyi,[46] T.Ferguson,[37] D.Fernandez,[28] F.Ferroni,[39] H.Fesefeldt,[1] E.Fiandrini,[36] J.H.Field,[21] F.Filthaut,[37] P.H.Fisher,[17] G.Forconi,[17] L.Fredj,[21] K.Freudenreich,[51] C.Furetta,[29] Yu.Galaktionov,[30,17] S.N.Ganguli,[11] P.Garcia-Abia,[28] S.S.Gau,[13] S.Gentile,[39] N.Gheordanescu,[14] S.Giagu,[39] S.Goldfarb,[24] J.Goldstein,[12] Z.F.Gong,[22] A.Gougas,[5] G.Gratta,[35] M.W.Gruenewald,[9] V.K.Gupta,[38] A.Gurtu,[11] L.J.Gutay,[48] B.Hartmann,[1] A.Hasan,[32] D.Hatzifotiadou,[10] T.Hebbeker,[9] A.Hervé,[19] W.C.van Hoek,[33] H.Hofer,[51] H.Hoorani,[37] S.R.Hou,[53] G.Hu,[5] V.Innocente,[19] K.Jenkes,[1] B.N.Jin,[8] L.W.Jones,[3] P.de Jong,[19] I.Josa-Mutuberria,[28] A.Kasser,[24] R.A.Khan,[20] D.Kamrad,[50] Yu.Kamyshkov,[34] J.S.Kapustinsky,[26] Y.Karyotakis,[4] M.Kaur,[20,◇] M.N.Kienzle-Focacci,[21] D.Kim,[5] J.K.Kim,[45] S.C.Kim,[45] Y.G.Kim,[45] W.W.Kinnison,[26] A.Kirkby,[35] D.Kirkby,[35] J.Kirkby,[19] D.Kiss,[15] W.Kittel,[33] A.Klimentov,[17,30] A.C.König,[33] I.Korolko,[30] V.Koutsenko,[17,30] R.W.Kraemer,[37] W.Krenz,[1] A.Kunin,[17,30] P.Ladron de Guevara,[28] I.Laktineh,[27] G.Landi,[18] C.Lapoint,[17] K.Lassila-Perini,[51] P.Laurikainen,[23] M.Lebeau,[19] A.Lebedev,[17] P.Lebrun,[27] P.Lecomte,[51] P.Lecoq,[19] P.Le Coultre,[51] J.S.Lee,[45] K.Y.Lee,[45] J.M.Le Goff,[19] R.Leiste,[50] E.Leonardi,[39] P.Levtchenko,[40] C.Li,[22] E.Lieb,[50] W.T.Lin,[53] F.L.Linde,[2,19] L.Lista,[31] Z.A.Liu,[8] W.Lohmann,[50] E.Longo,[39] W.Lu,[35] Y.S.Lu,[8] K.Lübelsmeyer,[1] C.Luci,[39] D.Luckey,[17] L.Luminari,[39] W.Lustermann,[49] W.G.Ma,[22] M.Maity,[11] G.Majumder,[11] L.Malgeri,[39] A.Malinin,[30] C.Maña,[28] D.Mangeol,[33] S.Mangla,[11] P.Marchesini,[51] A.Marin,[12] J.P.Martin,[27] F.Marzano,[39] G.G.G.Massaro,[2] D.McNally,[19] R.R.McNeil,[7] S.Mele,[31] L.Merola,[31] M.Meschini,[18] W.J.Metzger,[33] M.von der Mey,[1] Y.Mi,[24] A.Mihul,[14] A.J.W.van Mil,[33] G.Mirabelli,[39] J.Mnich,[19] P.Molnar,[9] B.Monteleoni,[18] R.Moore,[3] S.Morganti,[39] T.Moulik,[11] R.Mount,[35] S.Müller,[1] F.Muheim,[21] A.J.M.Muijs,[2] E.Nagy,[15] S.Nahn,[17] M.Napolitano,[31] F.Nessi-Tedaldi,[51] H.Newman,[35] T.Niessen,[1] A.Nippe,[1] A.Nisati,[39] H.Nowak,[50] H.Opitz,[1] G.Organtini,[39] R.Ostonen,[23] D.Pandoulas,[1] S.Paoletti,[39] P.Paolucci,[31] H.K.Park,[37] G.Pascale,[39] G.Passaleva,[18] S.Patricelli,[31] T.Paul,[13] M.Pauluzzi,[36] C.Paus,[1] F.Pauss,[51] D.Peach,[19] Y.J.Pei,[1] S.Pensotti,[29] D.Perret-Gallix,[4] B.Petersen,[33] S.Petrak,[9] A.Pevsner,[5] D.Piccolo,[31] M.Pieri,[18] J.C.Pinto,[37] P.A.Piroué,[38] E.Pistolesi,[29] V.Plyaskin,[30] M.Pohl,[51] V.Pojidaev,[30,18] H.Postema,[17] N.Produit,[21] D.Prokofiev,[40] G.Rahal-Callot,[51] P.G.Rancoita,[29] M.Rattaggi,[29] G.Raven,[42] P.Razis,[32]K.Read,[34] D.Ren,[51] M.Rescigno,[39] S.Reucroft,[13] T.van Rhee,[47] S.Riemann,[50] K.Riles,[3] S.Ro,[45] A.Robohm,[51] J.Rodin,[17] F.J.Rodriguez,[28] B.P.Roe,[3] L.Romero,[28] S.Rosier-Lees,[4] Ph.Rosselet,[24] W.van Rossum,[47] S.Roth,[1] J.A.Rubio,[19] H.Rykaczewski,[51] J.Salicio,[19] E.Sanchez,[28] M.P.Sanders,[33] A.Santocchia,[36] M.E.Sarakinos,[23] S.Sarkar,[11] M.Sassowsky,[1] C.Schäfer,[1] V.Schegelsky,[40] S.Schmidt-Kaerst,[1] D.Schmitz,[1] P.Schmitz,[1] N.Scholz,[51] H.Schopper,[52] D.J.Schotanus,[33] J.Schwenke,[1] G.Schwering,[1] C.Sciacca,[31] D.Sciarrino,[21] L.Servoli,[36] S.Shevchenko,[35] N.Shivarov,[44] V.Shoutko,[30] J.Shukla,[26] E.Shumilov,[30] A.Shvorob,[35] T.Siedenburg,[1] D.Son,[45] A.Sopczak,[50] B.Smith,[17] P.Spillantini,[18] M.Steuer,[17] D.P.Stickland,[38] H.Stone,[38] B.Stoyanov,[44] A.Straessner,[1] K.Strauch,[16] K.Sudhakar,[11] G.Sultanov,[20] L.Z.Sun,[22] G.F.Susinno,[21] H.Suter,[51] J.D.Swain,[20] X.W.Tang,[8] L.Tauscher,[6] L.Taylor,[13] Samuel C.C.Ting,[17] S.M.Ting,[17] M.Tonutti,[1] S.C.Tonwar,[11] J.Tóth,[15] C.Tully,[38] H.Tuchscherer,[46] K.L.Tung,[8]Y.Uchida,[17] J.Ulbricht,[51] U.Uwer,[19] E.Valente,[39] R.T.Van de Walle,[33] G.Vesztergombi,[15] I.Vetlitsky,[30] G.Viertel,[51] M.Vivargent,[4] R.Völkert,[50] H.Vogel,[37] H.Vogt,[50] I.Vorobiev,[30] A.A.Vorobyov,[40] A.Vorvolakos,[32] M.Wadhwa,[6] W.Wallraff,[1] J.C.Wang,[17] X.L.Wang,[22] Z.M.Wang,[22] A.Weber,[1] F.Wittgenstein,[19] S.X.Wu,[20] S.Wynhoff,[1] J.Xu,[12] Z.Z.Xu,[22] B.Z.Yang,[22] C.G.Yang,[8] X.Y.Yao,[8] J.B.Ye,[22] S.C.Yeh,[53] J.M.You,[37] An.Zalite,[40] Yu.Zalite,[40] P.Zemp,[51] Y.Zeng,[1] Z.Zhang,[8] Z.P.Zhang,[22] B.Zhou,[12] G.Y.Zhu,[8] R.Y.Zhu,[35] A.Zichichi,[10,19,20] F.Ziegler.[50]

1 I. Physikalisches Institut, RWTH, D-52056 Aachen, FRG[§]
III. Physikalisches Institut, RWTH, D-52056 Aachen, FRG[§]
2 National Institute for High Energy Physics, NIKHEF, and University of Amsterdam, NL-1009 DB Amsterdam, The Netherlands
3 University of Michigan, Ann Arbor, MI 48109, USA
4 Laboratoire d'Annecy-le-Vieux de Physique des Particules, LAPP,IN2P3-CNRS, BP 110, F-74941 Annecy-le-Vieux CEDEX, France
5 Johns Hopkins University, Baltimore, MD 21218, USA
6 Institute of Physics, University of Basel, CH-4056 Basel, Switzerland
7 Louisiana State University, Baton Rouge, LA 70803, USA
8 Institute of High Energy Physics, IHEP, 100039 Beijing, China[△]
9 Humboldt University, D-10099 Berlin, FRG[§]
10 University of Bologna and INFN-Sezione di Bologna, I-40126 Bologna, Italy
11 Tata Institute of Fundamental Research, Bombay 400 005, India
12 Boston University, Boston, MA 02215, USA
13 Northeastern University, Boston, MA 02115, USA
14 Institute of Atomic Physics and University of Bucharest, R-76900 Bucharest, Romania
15 Central Research Institute for Physics of the Hungarian Academy of Sciences, H-1525 Budapest 114, Hungary[‡]
16 Harvard University, Cambridge, MA 02139, USA
17 Massachusetts Institute of Technology, Cambridge, MA 02139, USA
18 INFN Sezione di Firenze and University of Florence, I-50125 Florence, Italy
19 European Laboratory for Particle Physics, CERN, CH-1211 Geneva 23, Switzerland
20 World Laboratory, FBLJA Project, CH-1211 Geneva 23, Switzerland
21 University of Geneva, CH-1211 Geneva 4, Switzerland
22 Chinese University of Science and Technology, USTC, Hefei, Anhui 230 029, China[△]
23 SEFT, Research Institute for High Energy Physics, P.O. Box 9, SF-00014 Helsinki, Finland
24 University of Lausanne, CH-1015 Lausanne, Switzerland
25 INFN-Sezione di Lecce and Universitá Degli Studi di Lecce, I-73100 Lecce, Italy
26 Los Alamos National Laboratory, Los Alamos, NM 87544, USA
27 Institut de Physique Nucléaire de Lyon, IN2P3-CNRS,Université Claude Bernard, F-69622 Villeurbanne, France
28 Centro de Investigaciones Energeticas, Medioambientales y Tecnologicas, CIEMAT, E-28040 Madrid, Spain♭
29 INFN-Sezione di Milano, I-20133 Milan, Italy
30 Institute of Theoretical and Experimental Physics, ITEP, Moscow, Russia
31 INFN-Sezione di Napoli and University of Naples, I-80125 Naples, Italy
32 Department of Natural Sciences, University of Cyprus, Nicosia, Cyprus
33 University of Nijmegen and NIKHEF, NL-6525 ED Nijmegen, The Netherlands
34 Oak Ridge National Laboratory, Oak Ridge, TN 37831, USA
35 California Institute of Technology, Pasadena, CA 91125, USA
36 INFN-Sezione di Perugia and Universitá Degli Studi di Perugia, I-06100 Perugia, Italy
37 Carnegie Mellon University, Pittsburgh, PA 15213, USA
38 Princeton University, Princeton, NJ 08544, USA
39 INFN-Sezione di Roma and University of Rome, "La Sapienza", I-00185 Rome, Italy
40 Nuclear Physics Institute, St. Petersburg, Russia
41 University and INFN, Salerno, I-84100 Salerno, Italy
42 University of California, San Diego, CA 92093, USA
43 Dept. de Fisica de Particulas Elementales, Univ. de Santiago, E-15706 Santiago de Compostela, Spain
44 Bulgarian Academy of Sciences, Central Lab. of Mechatronics and Instrumentation, BU-1113 Sofia, Bulgaria
45 Center for High Energy Physics, Korea Adv. Inst. of Sciences and Technology, 305-701 Taejon, Republic of Korea
46 University of Alabama, Tuscaloosa, AL 35486, USA
47 Utrecht University and NIKHEF, NL-3584 CB Utrecht, The Netherlands
48 Purdue University, West Lafayette, IN 47907, USA
49 Paul Scherrer Institut, PSI, CH-5232 Villigen, Switzerland
50 DESY-Institut für Hochenergiephysik, D-15738 Zeuthen, FRG
51 Eidgenössische Technische Hochschule, ETH Zürich, CH-8093 Zürich, Switzerland
52 University of Hamburg, D-22761 Hamburg, FRG
53 High Energy Physics Group, Taiwan, China
§ Supported by the German Bundesministerium für Bildung, Wissenschaft, Forschung und Technologie
‡ Supported by the Hungarian OTKA fund under contract number T14459.
♭ Supported also by the Comisión Interministerial de Ciencia y Technología
♯ Also supported by CONICET and Universidad Nacional de La Plata, CC 67, 1900 La Plata, Argentina
◊ Also supported by Panjab University, Chandigarh-160014, India
△ Supported by the National Natural Science Foundation of China.

$\mathbf{e^+e^-\to} \boldsymbol{qqe\nu(\gamma)}$		
Selection Efficiencies [%]	$qqe\nu(\gamma)$	76.3
	$qq\tau\nu(\gamma)$	1.4
Non-W Background [fb]		15.5
Total Systematic Uncertainty [%]		$\pm$ 5

$\mathbf{e^+e^-\to} \boldsymbol{qq\mu\nu(\gamma)}$		
Selection Efficiencies [%]	$qq\mu\nu(\gamma)$	66.0
	$qq\tau\nu(\gamma)$	2.1
Non-W Background [fb]		16.2
Total Systematic Uncertainty [%]		$\pm$ 5

$\mathbf{e^+e^-\to} \boldsymbol{qq\tau\nu(\gamma)}$		
Selection Efficiencies [%]	$qq\tau\nu(\gamma)$	37.5
	$qqe\nu(\gamma)$	4.7
	$qq\mu\nu(\gamma)$	4.8
	$qqqq(\gamma)$	0.1
Non-W Background [fb]		157.
Total Systematic Uncertainty [%]		$\pm$20

$\mathbf{e^+e^-\to} \boldsymbol{\ell\nu\ell\nu(\gamma)}$		
Selection Efficiency [%]	$\ell\nu\ell\nu(\gamma)$	39.8
Non-W Background [fb]		40.3
Total Systematic Uncertainty [%]		$\pm$ 5

Table 1: Selection efficiencies, accepted background cross sections from non-W processes, and total systematic uncertainties for signal processes $e^+e^- \to qqe\nu(\gamma)$, $e^+e^- \to qq\mu\nu(\gamma)$, $e^+e^- \to qq\tau\nu(\gamma)$, $e^+e^- \to \ell\nu\ell\nu(\gamma)$. For the $qqe\nu$ signal, the signal efficiency is derived from a CC20 Monte Carlo sample and is given within cuts, see Section 3.1. For the $\ell\nu\ell\nu$ signal, the signal efficiency is derived from a CC56+NC56 Monte Carlo sample and is given within cuts, see Section 3.4. The total systematic uncertainties are relative to the cross sections listed in Table 2. For the $qq\tau\nu$ signal, the systematic error is dominated by finite Monte Carlo statistics of the $q\bar{q}(\gamma)$ background.

Process	$\mathcal{L}$ [pb^{-1}]	$N_{\rm data}$	$N_{\rm bg}$	σ(cuts) [pb]	σ(CC03) [pb]	$r_{\rm SM}$ [%]	$\sigma_{\rm SM}$ [pb]
$\mathrm{e^+e^-} \to qq\mathrm{e}\nu(\gamma)$	10.2	4	0.16	$0.49^{+0.30}_{-0.22}$	$0.62^{+0.38}_{-0.27}$	14.6	0.56
$\mathrm{e^+e^-} \to qq\mu\nu(\gamma)$	10.9	4	0.18	—	$0.53^{+0.33}_{-0.24}$	14.6	0.56
$\mathrm{e^+e^-} \to qq\tau\nu(\gamma)$	10.2	3	1.61	—	$0.22^{+0.55}_{-0.38}$	14.6	0.56
$\mathrm{e^+e^-} \to \ell\nu\ell\nu(\gamma)$	9.6	2	0.39	$0.42^{+0.46}_{-0.29}$	$0.39^{+0.43}_{-0.27}$	10.6	0.41
$\mathrm{e^+e^-} \to qqqq(\gamma)$	10.2	8.9	—	—	$0.98^{+0.51}_{-0.40}$	45.6	1.76

Table 2: Total luminosity used in the analyses, $\mathcal{L}$, number of selected data events, $N_{\rm data}$, number of expected non-W background events, $N_{\rm bg}$, and cross sections for the reactions $\mathrm{e^+e^-} \to qq\mathrm{e}\nu(\gamma)$, $\mathrm{e^+e^-} \to qq\mu\nu(\gamma)$, $\mathrm{e^+e^-} \to qq\tau\nu(\gamma)$, $\mathrm{e^+e^-} \to \ell\nu\ell\nu(\gamma)$ and $\mathrm{e^+e^-} \to qqqq(\gamma)$. For the $qq\mathrm{e}\nu$ and $\ell\nu\ell\nu$ signal, the cross sections within the cuts described in Sections 3.1 and 3.4, σ(cuts), are given in addition to the CC03 cross sections, σ(CC03). For the $qqqq$ final state, the number of events is calculated using luminosity, signal efficiency, and signal cross section as derived in the fit described in Section 3.5. Also shown are the CC03 branching fractions, $r_{\rm SM}$, and the CC03 cross sections, $\sigma_{\rm SM}$, as expected within the Standard Model. They are calculated using Standard-Model W-decay branching fractions [3] and the GENTLE [25] program for a W mass of 80.33 GeV [5]. The errors are statistical only.

Parameter	Lepton Non-Universality	Lepton Universality	Standard Model
$B(\mathrm{W}\rightarrow \mathrm{e}\nu)$ [%]	$18^{+11}_{-\ 8}$	—	
$B(\mathrm{W}\rightarrow \mu\nu)$ [%]	$16^{+10}_{-\ 7}$	—	
$B(\mathrm{W}\rightarrow \tau\nu)$ [%]	6^{+12}_{-11}	—	
$B(\mathrm{W}\rightarrow \ell\nu)$ [%]	—	$13^{+\ 3}_{-\ 3}$	10.8
$B(\mathrm{W}\rightarrow qq)$ [%]	61^{+10}_{-11}	$60^{+\ 9}_{-10}$	67.5
σ_{WW} [pb]	$2.73^{+0.87}_{-0.74}$	$2.94^{+0.84}_{-0.72}$	3.85

Parameter	Using SM W-Decay Branching Fractions	Standard Model
σ_{WW} [pb]	$2.89^{+0.81}_{-0.70}$	3.85

Table 3: W-decay branching fractions, B, and total W-pair cross section, σ_{WW}, derived with and without the assumption of charged-current lepton universality. In the bottom part of the table, the measured total W-pair cross section imposing Standard-Model W-decay branching fractions is given. The errors are statistical only. Also shown are the W-decay branching fractions [3] and the total W-pair cross section as expected in the Standard Model. The latter is calculated for $\mathrm{M_W} = 80.33$ GeV [5] using the GENTLE [25] program.

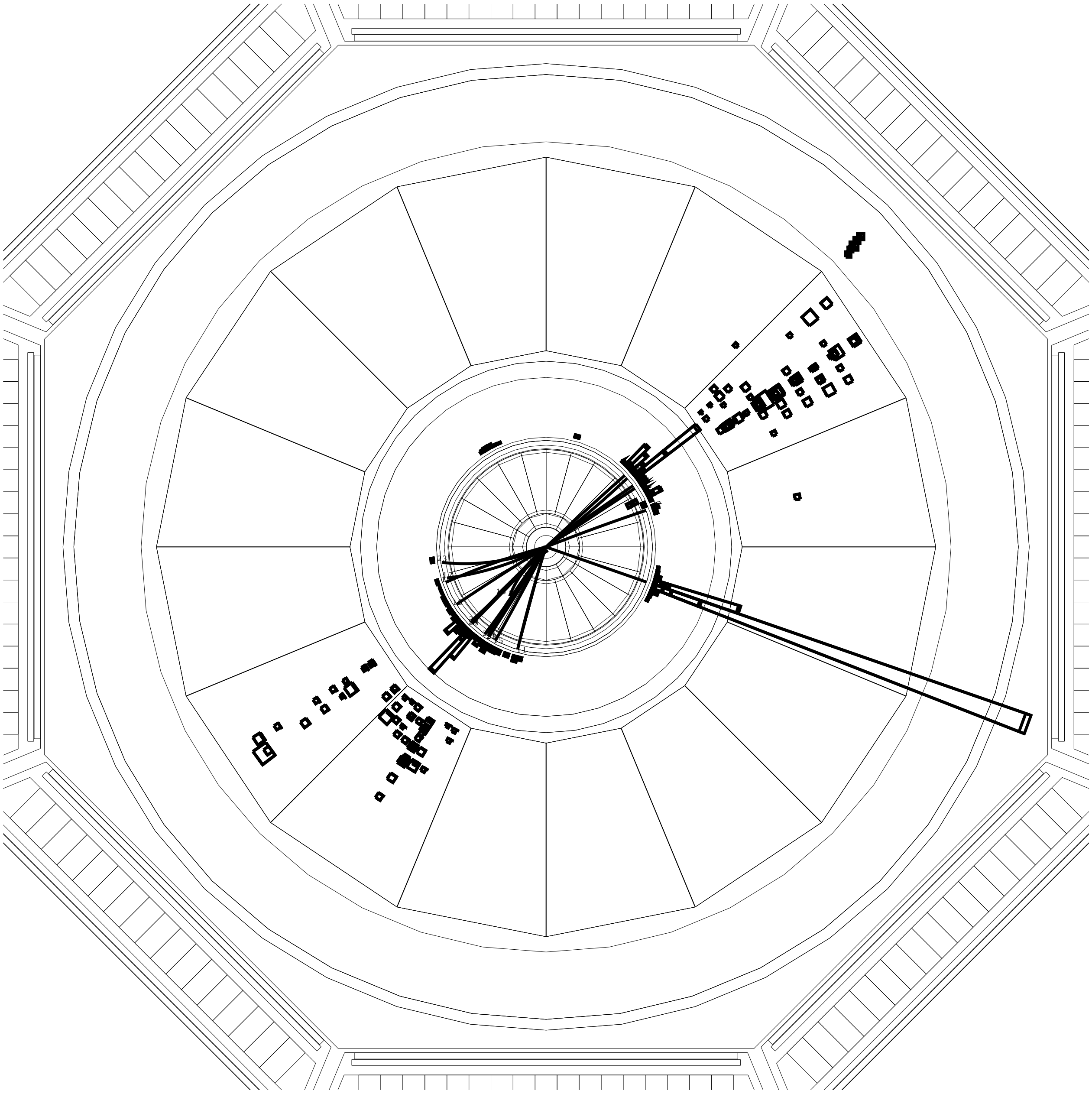

Figure 1: A $qqe\nu$ event selected in the data. Shown is the view in the plane perpendicular to the beam axis. The thick lines are the tracks reconstructed in the central tracking chamber. Energy depositions in the electromagnetic and hadron calorimeter are shown as squares with size proprotional to the amount of energy deposited in the calorimeter cell. The large cluster to the right in the electromagnetic calorimeter with a track pointing to it is identified as the electron. The two hadronic jets correspond to the qq system. The kinematic quantities of this event are measured to be: $E_{\mathrm{e}} = 36$ GeV, $E_{\nu} = 45$ GeV, $M_{qq} = 90$ GeV and $M_{\mathrm{e}\nu} = 80$ GeV.

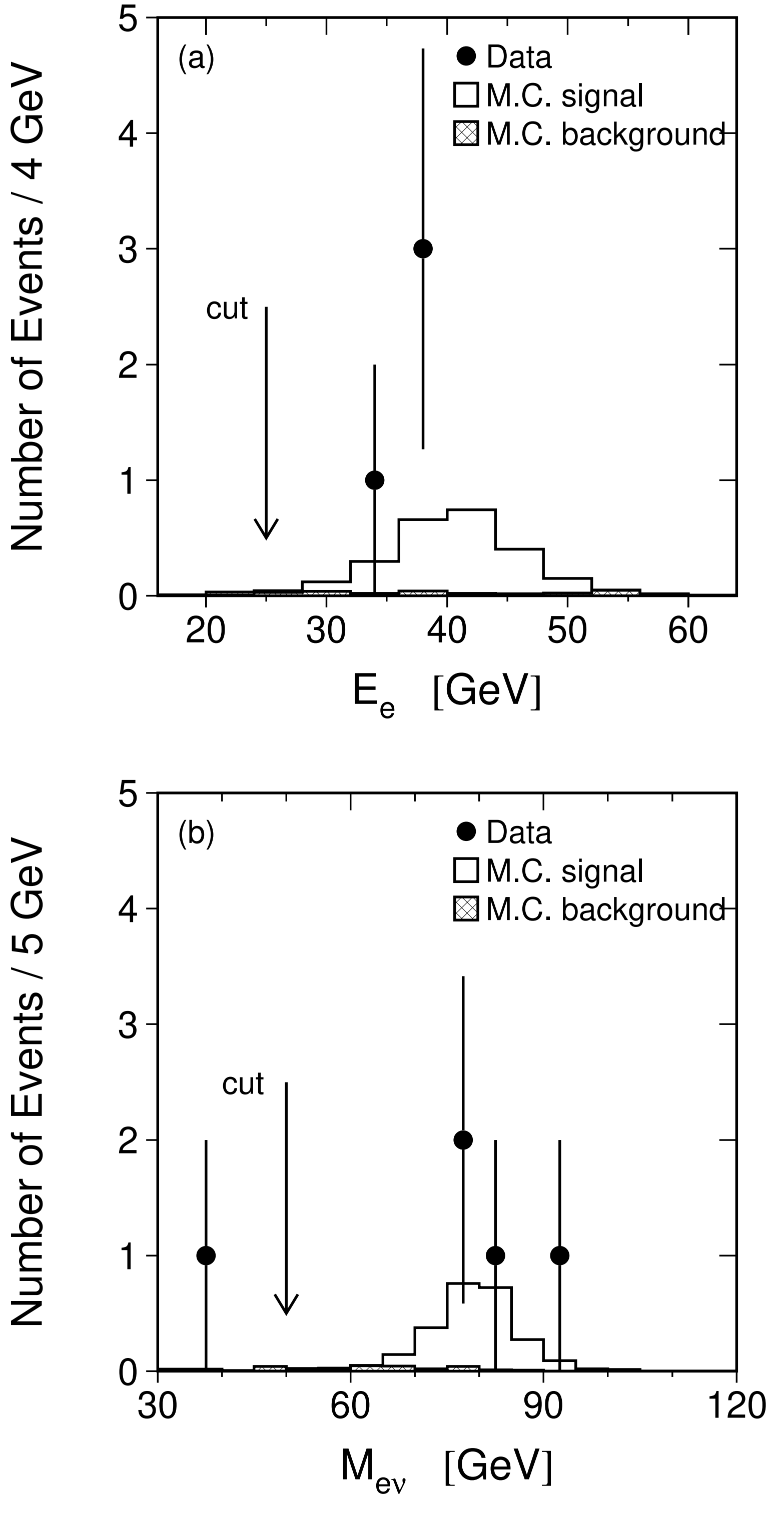

Figure 2: Distributions of variables used for the selection of $e^+e^- \rightarrow qqe\nu(\gamma)$ events, comparing the data to the signal and background Monte Carlo. The position of the selection cuts are indicated by vertical arrows. All selection cuts except in the variable plotted are applied. (a) The electron energy, E_e. (b) The invariant mass of the electron-neutrino system, $M_{e\nu}$. For this channel the background is negligible.

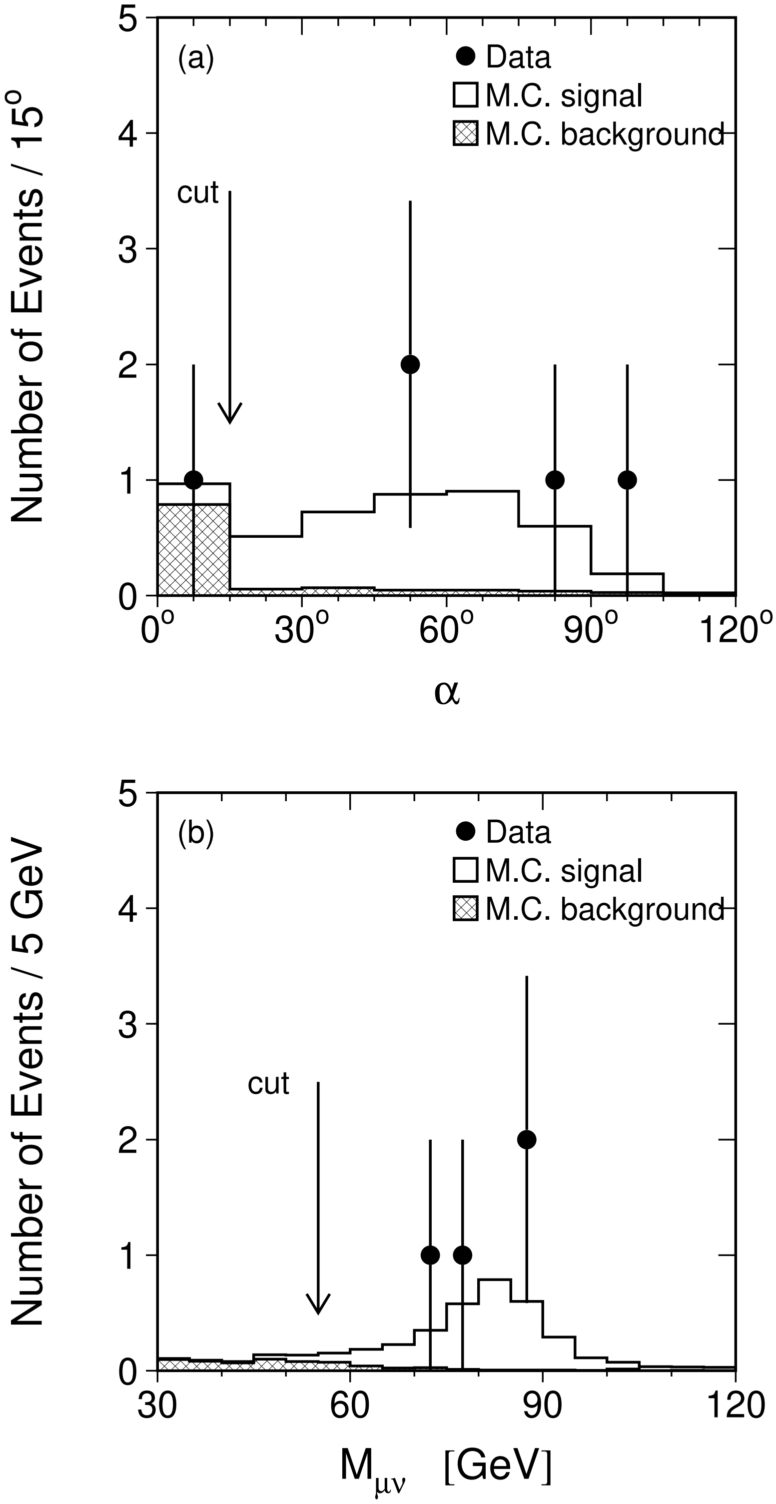

Figure 3: Distributions of variables used for the selection of $e^+e^- \to qq\mu\nu(\gamma)$ events, comparing the data to the signal and background Monte Carlo. The position of the selection cuts are indicated by vertical arrows. All selection cuts except in the variable plotted are applied. (a) The angle of the muon to the nearest jet, α. (b) The invariant mass of the muon-neutrino system, $M_{\mu\nu}$.

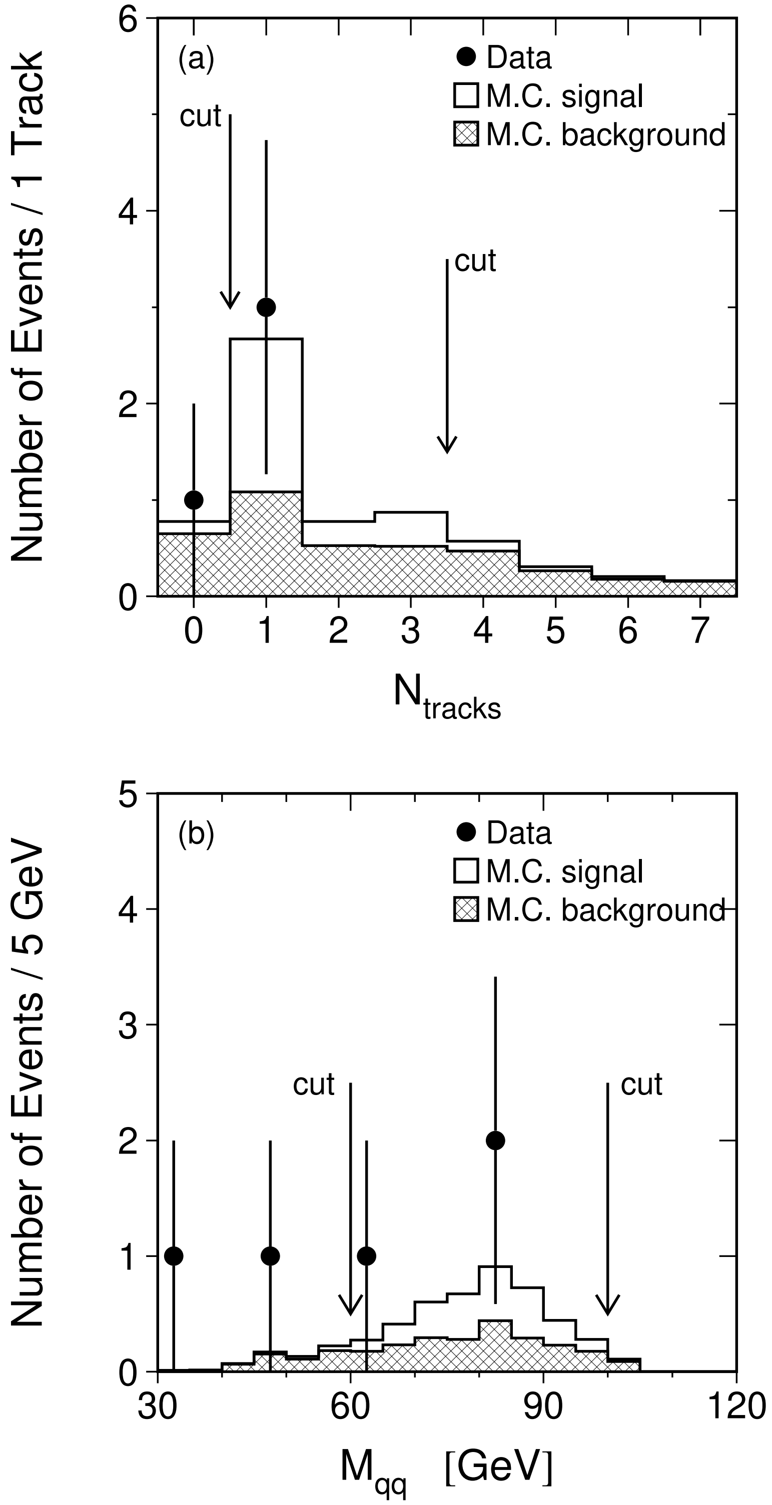

Figure 4: Distributions of variables used for the selection of $\mathrm{e}^+\mathrm{e}^- \to qq\tau\nu(\gamma)$ events, comparing the data to the signal and background Monte Carlo. The position of the selection cuts are indicated by vertical arrows. All selection cuts except in the variable plotted are applied. (a) The number of tracks reconstructed in the central tracking chamber and associated with the tau jet, N_{tracks}. (b) The invariant mass of the jet-jet system, M_{qq}.

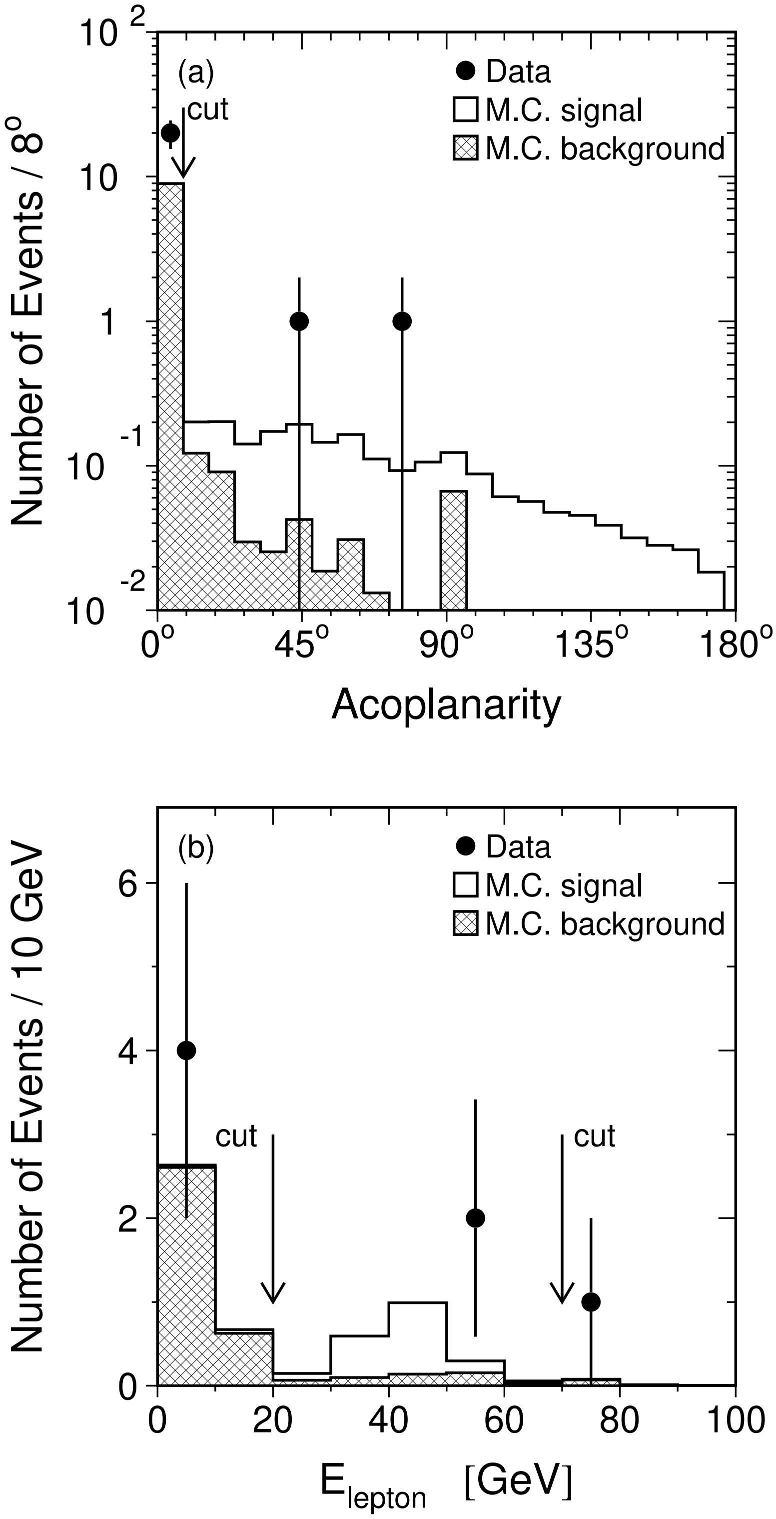

Figure 5: Distributions of variables used for the selection of $e^+e^- \rightarrow \ell\nu\ell\nu(\gamma)$ events, comparing the data to the signal and background Monte Carlo. The position of the selection cuts are indicated by vertical arrows. All selection cuts except in the variable plotted are applied. (a) Acoplanarity between the two charged leptons. The excess in the first bin arises from cosmic-ray background. (b) Energy of identified electron or muon with highest energy, E_{lepton}.

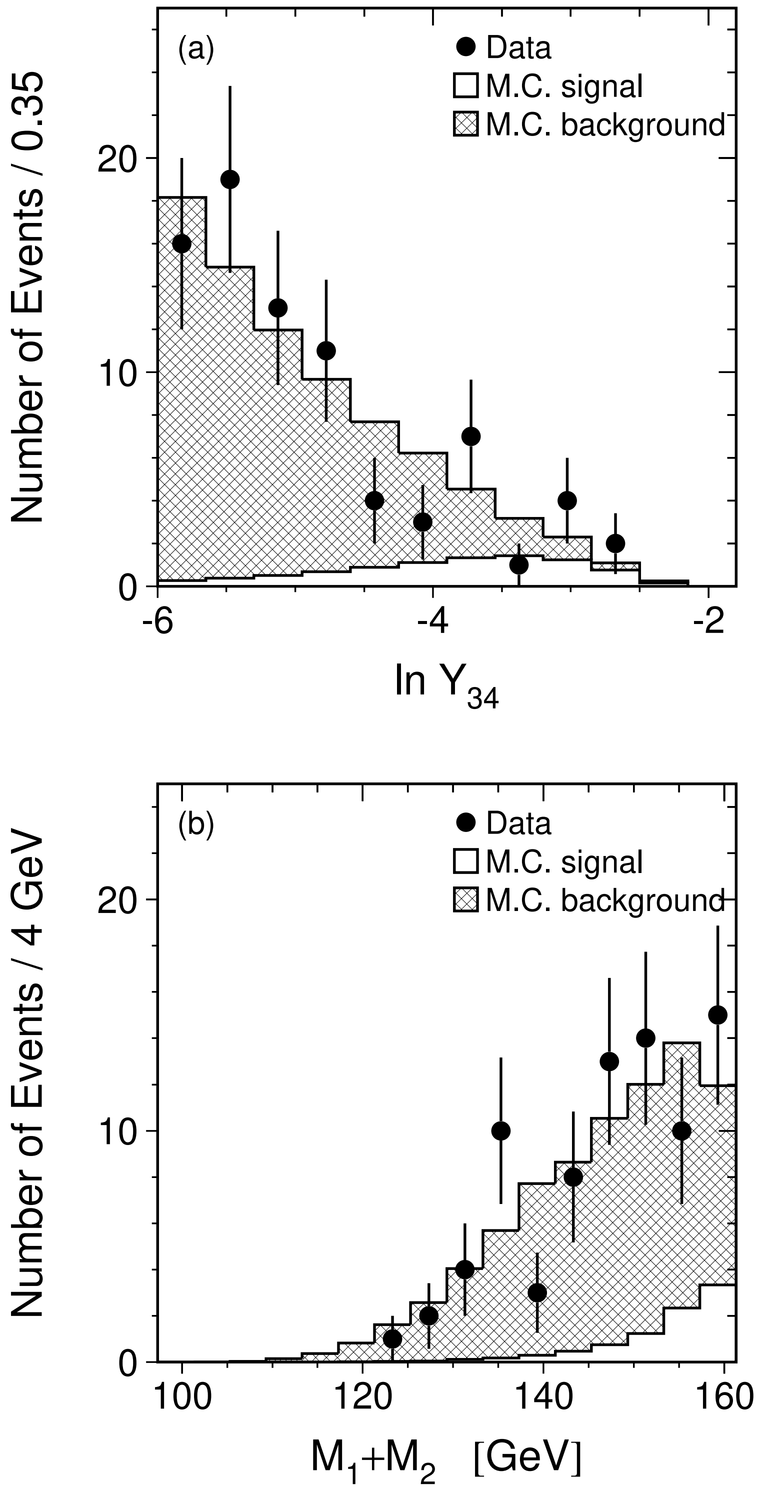

Figure 6: Distributions of variables used for the neural network in the analysis of $e^+e^- \to qqqq(\gamma)$ events, comparing the data to the signal and background Monte Carlo. All selection cuts are applied. (a) The jet resolution parameter, Y_{34}. (b) The sum of the two jet-jet invariant masses, $M_1 + M_2$.

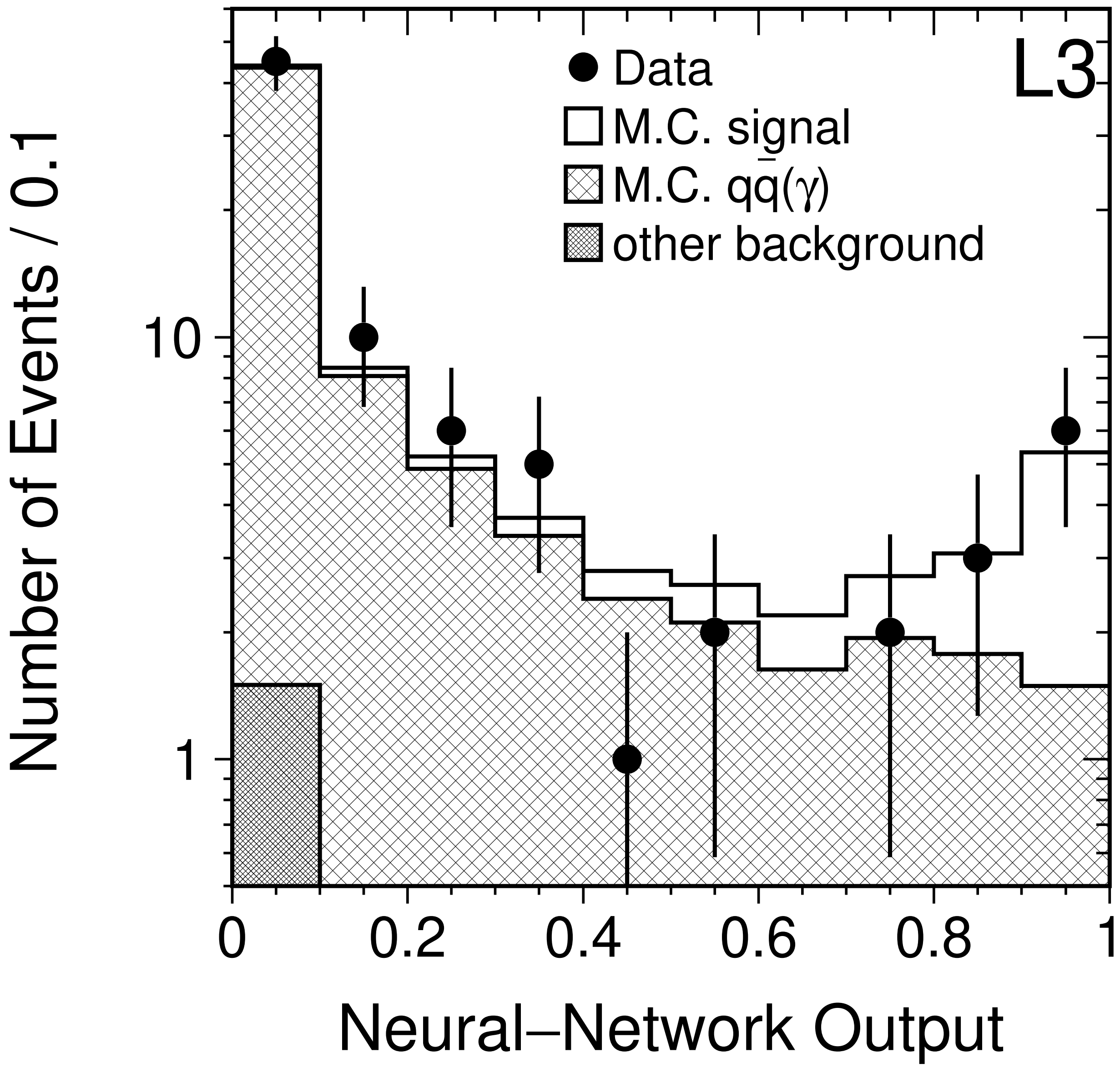

Figure 7: Distribution of the output of the neural network used in the analysis of $e^+e^- \rightarrow qqqq(\gamma)$ events, comparing the data to the signal and background Monte Carlo. All selection cuts are applied.

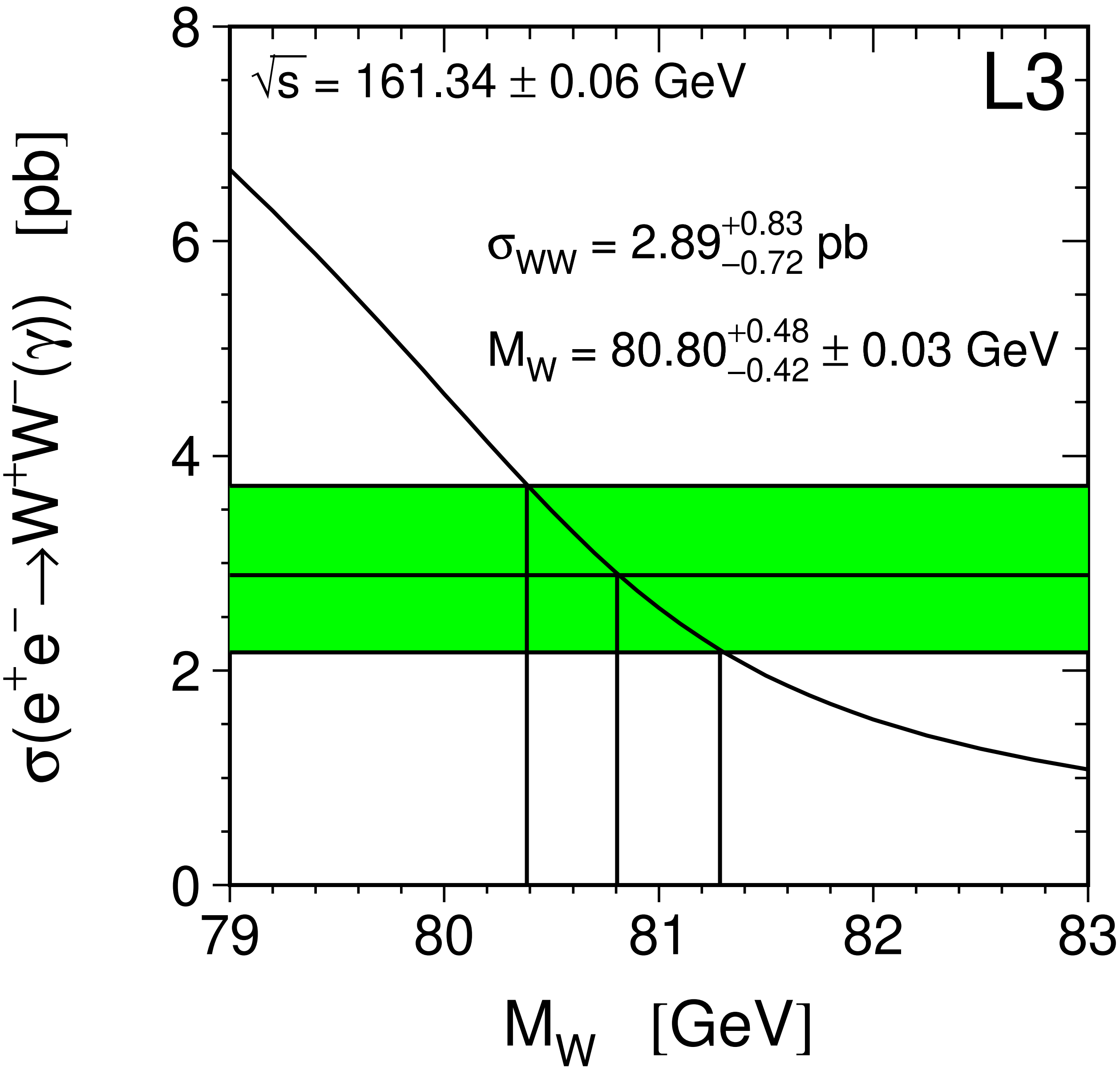

Figure 8: The cross section, σ_{WW}, of the process $\mathrm{e^+e^-} \to \mathrm{WW} \to ffff(\gamma)$ as a function of the W-mass, $\mathrm{M_W}$. The horizontal band shows the cross-section measurement with its total error, combining statistical and systematic error in quadrature. The curve shows the Standard Model expectation and is computed with the GENTLE [25] program. The second error on $\mathrm{M_W}$ arises from the LEP beam energy calibration [22].

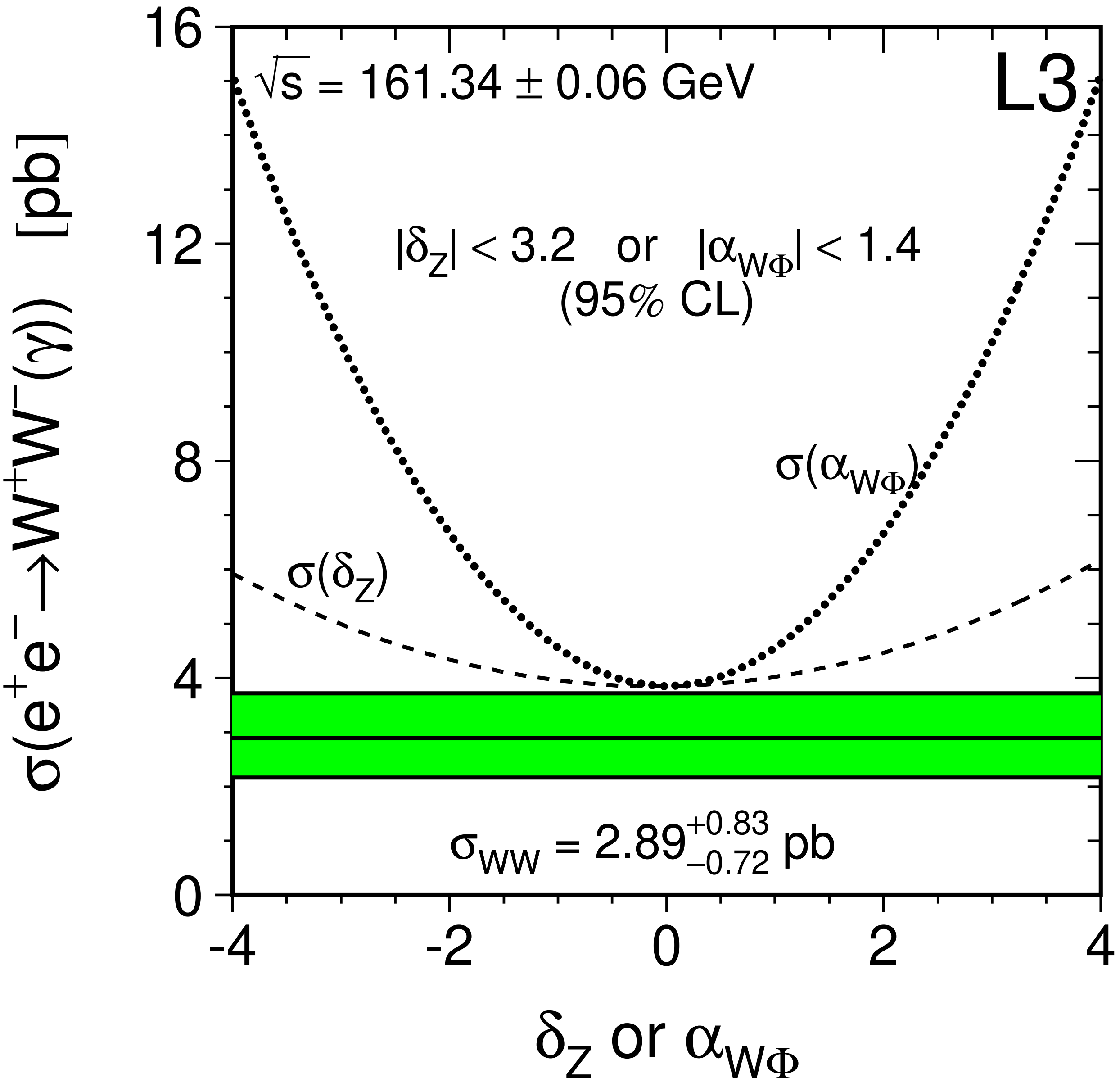

Figure 9: The cross section, $\sigma_{\rm WW}$, of the process $\rm e^+e^- \to WW \to \it ffff(\gamma)$ as a function of the anomalous triple-vector-boson couplings $\delta_{\rm Z}$ and $\alpha_{\rm W\Phi}$. The horizontal band shows the cross-section measurement with its total error, combining statistical and systematic error in quadrature. The dashed and dotted curves show the expectations for $\sigma(\delta_{\rm Z})$ and $\sigma(\alpha_{\rm W\Phi})$. They are calculated for $\rm M_W = 80.33$ GeV [5] using the GENTLE [25] program.